15th Canadian Masonry Symposium
Ottawa, Canada
June 2-5, 2025

Cyclic In-Plane Behavior of Masonry Infilled RC Frames with Detailed Interpretation of Damage Using Digital Image Correlation

Zeeshan Manzoor Bhat[i] and Yogendra Singh[ii]

ABSTRACT

This paper investigates the cyclic behavior of reinforced concrete (RC) frames with various types of masonry infills: burnt clay bricks, fly ash bricks, and autoclaved aerated concrete (AAC) blocks. The RC frames were designed in compliance with the latest provisions of the Indian seismic code. To assess the impact of masonry infills, four specimens-one bare frame and three masonry infilled frames-were subjected to cyclic loading. Digital Image Correlation (DIC) was employed to provide a detailed analysis of damage progression throughout the testing process. The study focused on key parameters such as stiffness, strength, and energy dissipation, and a comparison with available analytical models was conducted. Infilled frames were found to exhibit greater stiffness, strength, and energy dissipation compared to the bare frame. Due to the seismic code-compliant design, a ductile failure mode was observed in both the bare and infilled frames. The experimental results showed good agreement with certain analytical models regarding strength and stiffness. The infills restrained deformation at the base of the surrounding columns, resulting in dispersed flexural cracks in the columns, while cracks in the bare frame columns were concentrated at the base.

KEYWORDS

AAC block, cyclic testing, DIC, fly ash brick, masonry infill, RC frame

[i] Research Scholar, Department of Earthquake Engineering, IIT Roorkee, Roorkee, India, zbhat@eq.iitr.ac.in
[ii] Professor, Department of Earthquake Engineering, IIT Roorkee, Roorkee, India, yogendra.singh@eq.iitr.ac.in

INTRODUCTION

Unreinforced masonry (URM) infilled reinforced concrete (RC) frames are widely used as a structural system in many regions globally. Despite their prevalence, masonry infills are typically regarded as non-structural elements and are often neglected in the design and analysis of buildings. Post-earthquake reconnaissance has revealed that buildings with URM infilled RC frames are generally more susceptible to damage compared to RC frame buildings without infills [1-11]. This increased vulnerability is attributed to the masonry infills stiffening the structure, which results in higher seismic force demands. Additionally, these infills exert lateral forces on adjacent columns, potentially causing shear failure if the columns are not adequately designed to withstand these forces. The current Indian seismic code incorporates key safety provisions, such as the inclusion of special reinforcements at the ends of beams and columns, designing columns to be stronger than beams, and adopting capacity design principles. While these measures do not explicitly account for the influence of infills, they enhance the overall strength of the RC frame, which may help counteract the additional forces introduced by the infills. Therefore, investigating how these code provisions influence the seismic performance of URM infilled RC frames is essential for a deeper understanding of their behavior under earthquake loading.

The construction industry is increasingly prioritizing eco-friendly masonry options like fly ash bricks and autoclaved aerated concrete (AAC) blocks, as traditional burnt clay bricks are linked to high greenhouse gas emissions. The growing popularity of AAC blocks and fly ash bricks stems from their use of fly ash, an industrial by-product, as a key component. However, the structural behavior of these alternative materials compared to conventional burnt clay bricks requires further investigation. Experimental testing of masonry infills often involves manually marking cracks on the specimen's surface after each loading cycle, which is a labor-intensive and time-consuming process, particularly for full-scale tests. Moreover, this manual approach may overlook fine details of crack propagation, especially in brittle materials like masonry. To address these challenges, non-contact techniques such as Digital Image Correlation (DIC) provide a more accurate and efficient solution for damage monitoring.

This study investigates the performance of full-scale RC frames infilled with three types of masonry materials: burnt clay bricks, fly ash bricks, and AAC blocks. The RC frames were designed following the provisions of the current Indian seismic codes. The study emphasizes the impact of these infill materials on key parameters such as strength, stiffness, energy dissipation, and failure patterns. To gain detailed insights into crack propagation, damage progression, and the interaction between the masonry infills and the surrounding frames, DIC was utilized.

METHODOLOGY

Experimental Programme

Four full-scale specimens, representing the ground story of a typical five-story structure, were subjected to in-plane cyclic loading. The building was assumed to be located in the highest seismic hazard zone of India, Zone V (Zone factor = 0.36) equivalent to an Effective Peak Ground Acceleration of 0.54 g and was designed and detailed according to BIS 2000 [12] and BIS 2016 [13], which are consistent with modern international seismic design standards. Figure 1 shows a photograph of one of the specimens, including details of its reinforcement configuration. The columns had a longitudinal reinforcement ratio of 1.45%, while the beams had reinforcement ratios of 0.85% at the top and 0.53% at the bottom. Additionally, special

confining reinforcement was provided at the beam and column ends by using closed spaced stirrups up to a certain distance from the ends. To ensure a rigid foundation for the columns, a reinforced concrete base beam with dimensions of 550 × 550 mm was constructed. Among the specimens, one was a bare RC frame, while the remaining three included masonry infills made of burnt clay bricks, fly ash bricks, and AAC blocks, respectively.

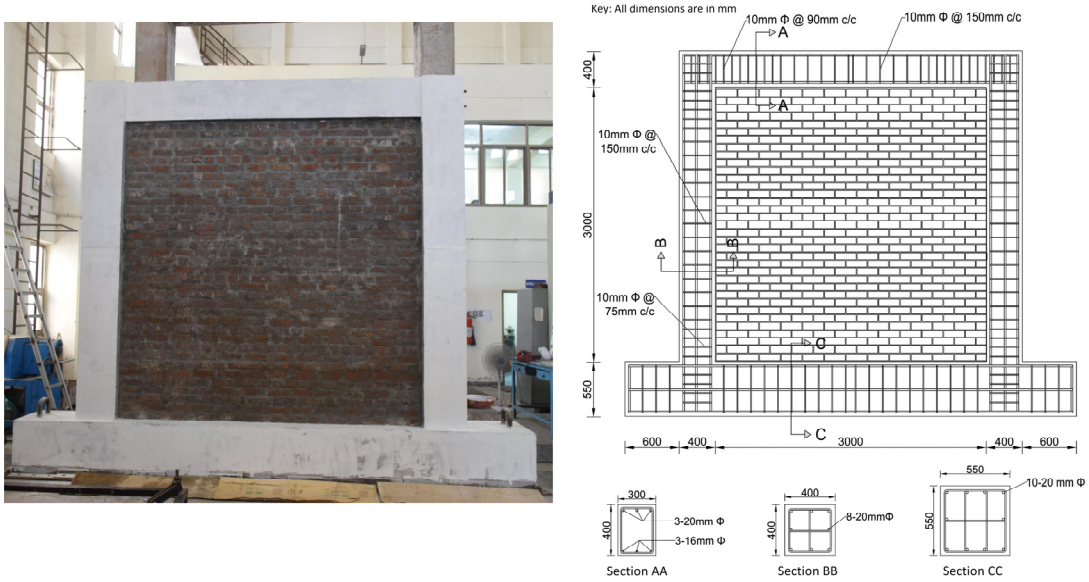

(a) (b)

Figure 1: (a) Burnt Clay Brick Masonry Infilled RC Frame; and (b) Reinforcement Detailing of the RC Frame.

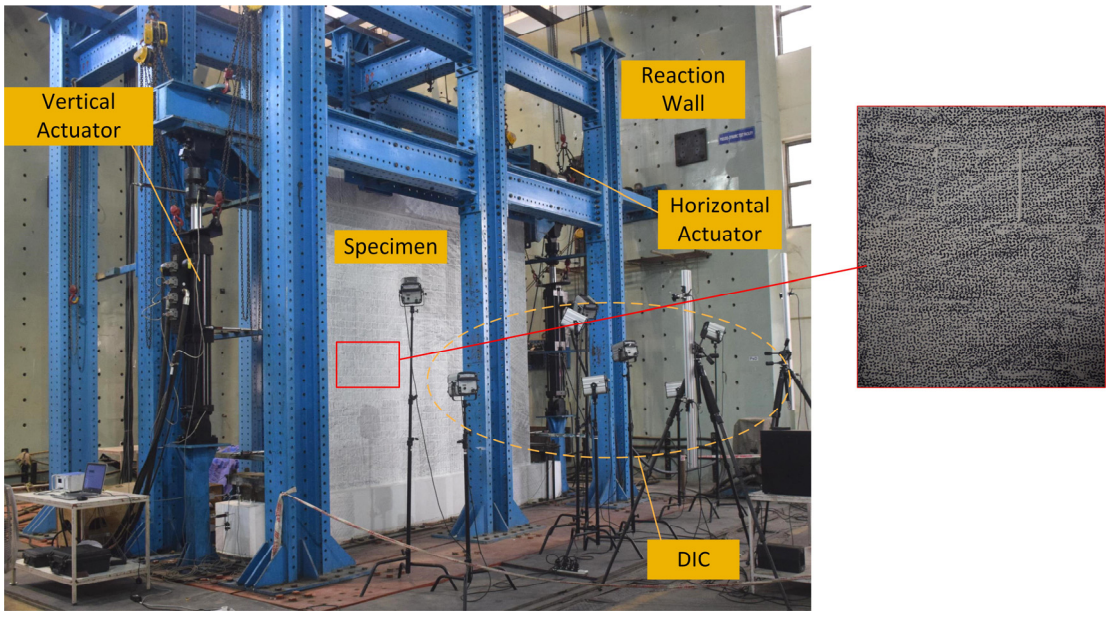

Figure 2: Test Setup for In-Plane Testing.

Figure 2 illustrates the specifics of the test setup. Cyclic loading was applied using a hydraulic actuator, following the guidelines outlined in ACI 2013 [14]. For each displacement increment, three cycles were applied, and the process was continued until either collapse occurred or a significant reduction in the

strength of the masonry infill was observed. A constant vertical load of 200 kN was applied to the columns using vertical actuators connected to a steel loading beam resting on the beam of the specimen. No vertical load was applied to the beam or infill. DIC was employed on the front side of the specimen to monitor deformation. DIC operates on the principle that surface characteristics of the specimen move with the object during deformation, maintaining their gray-level distribution before and after deformation. To determine displacement, the DIC algorithm identifies areas with the same gray-level distribution as prior to deformation [15]. A random speckle pattern was applied to the specimen's surface to facilitate this process, as shown in Figure 2. Four monochrome Basler Ace classic series cameras (acA1920-25) equipped with 16 mm focal length lenses and an 8-megapixel resolution (3840 × 2160 pixels) captured images at a rate of 10 frames per second. The images were then processed using VIC-3D software [16] to study the damage patterns. Detailed information about calibration and analysis procedures can be found in Bhat et al. [17]. In addition to DIC, lateral deformations were measured using linear variable displacement transducers (LVDTs) installed at multiple points along the column's height.

Material Properties

Masonry prisms and wallettes of the considered masonry infills were constructed and subjected to uniaxial compression and diagonal compression, respectively. The compressive strength and shear strength of the masonry assemblage, along with the elastic modulus and shear modulus, are summarized in Table 1. In addition to that, compression testing was conducted on individual masonry units and mortar. The compressive strength of burnt clay brick, fly ash brick, and AAC block was 19.5 MPa, 15.2 MPa, and 4.5 MPa, respectively. Similarly, the compressive strength of cement mortar in the case of burnt clay and fly ash brick masonry was 8.9 MPa, while adhesive mortar in the case of AAC block masonry had a compressive strength of 6.6 MPa. Further details regarding the mechanical characterization of these materials can be found in Bhat et al. [18].

Table 1: Mechanical Properties of the Masonry Used.

Masonry Type	Comp. strength (MPa)	Elastic modulus (MPa)	Shear strength (MPa)	Shear modulus (MPa)
Burnt clay brick	6.47	4100	0.92	1630
Fly ash brick	6.03	3582	0.84	1502
AAC block	4.08	2500	0.4	632

RESULTS AND DISCUSSION

Hysteretic Behavior

Figure 3 depicts the hysteretic behavior of all tested specimens, while Figure 4 presents the backbone curves for the specimens, including those of the bare frame and the infill-only case. The infill-only curve was derived by isolating the bare frame's contribution from the total strength of the masonry infilled frame. In the initial stages, the infill resisted a substantial portion of the lateral load compared to the surrounding frame. However, as the drift increased, the infill's contribution diminished, and by the end of the test, the frame alone carried the entire lateral load. This behavior is clearly depicted in Figure 4, where the backbone curve of the infilled frame converges with that of the bare frame toward the end of the test. Table 2 summarizes the parameters of all tested specimens. The strengths of the masonry infilled frames with burnt clay brick, fly ash brick, and AAC blocks were approximately 1.8, 1.84, and 1.5 times, respectively, greater than that of the bare frame. The lower strength observed in the AAC block masonry infilled frame is attributed to the relatively low compressive and shear strengths of AAC masonry.

The initial stiffness was evaluated using an idealized bilinear curve constructed in accordance with ASCE 2017 [19], in such a way that the areas under the actual backbone curve and the bilinearized curve were equivalent. Additionally, the initial line of the bilinearized curve was aligned to intersect the actual backbone curve at 60% of the yield strength. The initial stiffness of the masonry infilled frames with burnt clay brick, fly ash brick, and AAC blocks was approximately 12.8, 10, and 7 times, respectively, higher than that of the bare frame.

Figure 5 illustrates the variation in cumulative energy dissipation and stiffness with respect to drift. The burnt clay brick and fly ash brick masonry infilled frames exhibited similar energy dissipation capacities, while the AAC block masonry infilled frame displayed the lowest energy dissipation among the three. This reduced energy dissipation in the AAC block masonry infilled frame is attributed to its comparatively lower strength.

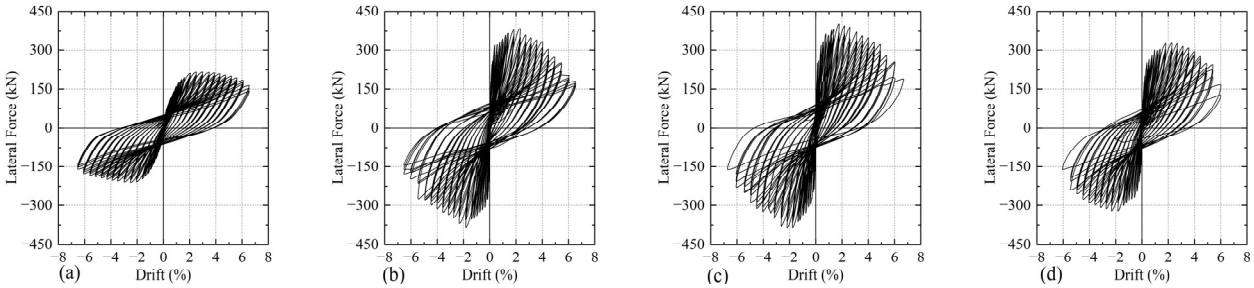

Figure 3: Hysteretic Behavior of : (a) Bare Frame (BF); (b) Burnt Clay Brick Masonry Infilled Frame (CB); (c) Fly Ash Brick Masonry Infilled Frame (FA); and (d) AAC Block Masonry Infilled Frame (AAC).

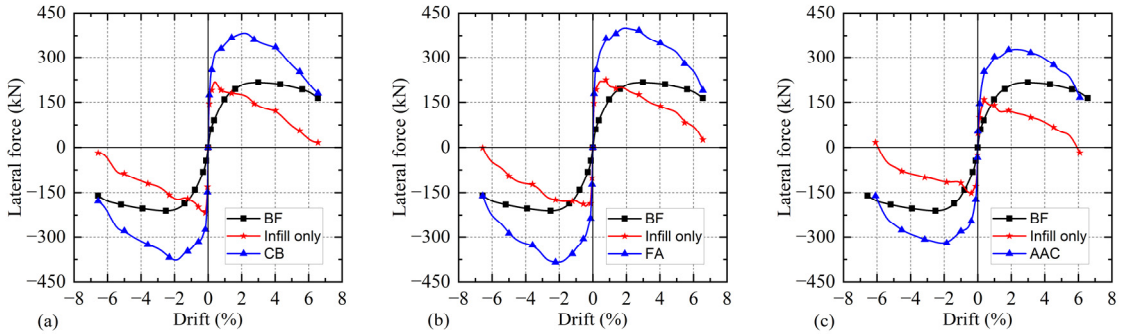

Figure 4: Backbone Curve of Masonry Infilled Frame and Masonry Infill Only of: (a) Burnt Clay Brick Masonry; (b) Fly Ash Brick Masonry; and (c) AAC Block Masonry.

Table 2: Properties of the Tested Specimens.

Specimen type	Peak strength (kN)	Drift corresponding to peak strength (%)	Initial stiffness (kN/mm)
BF	213.5	2.5	7.0
CB	385.0	2.0	89.7
FA	393.0	2.0	69.5
AAC	323.0	2.3	49.6

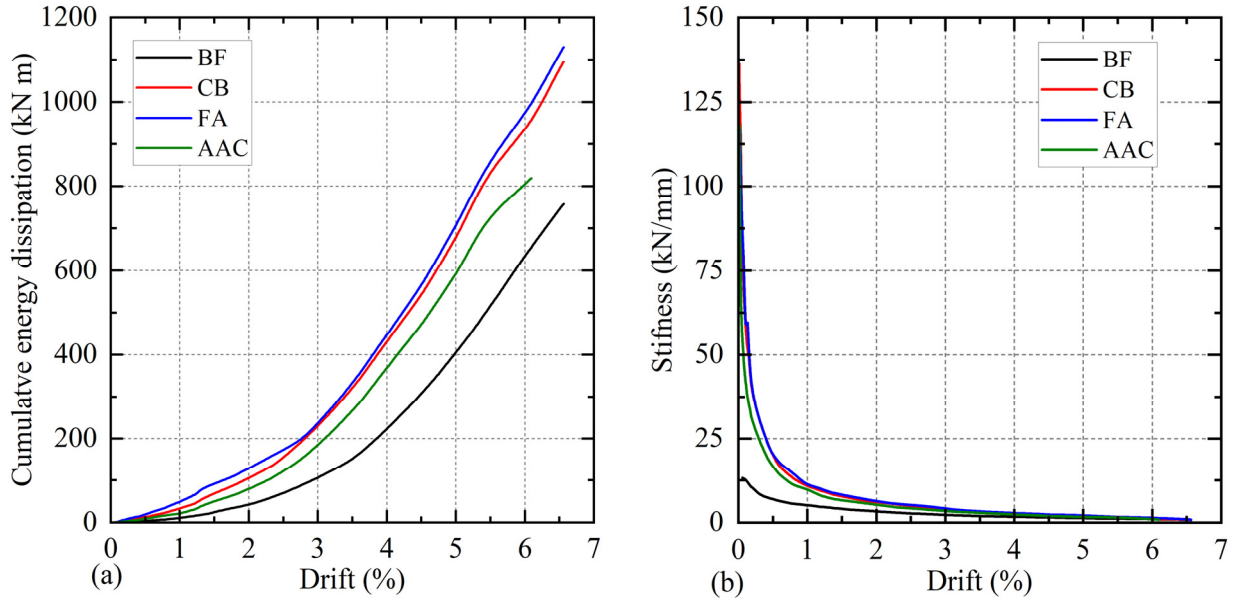

Figure 5: Variation of: (a) Cumulative Energy Dissipation; and (b) Stiffness Degradation with Increasing Drift.

Damage Visualization Using DIC

Figures 6–9 illustrate the damage patterns and the variation of principal strain for all the tested specimens. In the case of the bare frame, flexural cracks were intiated at the base of the columns and increased in both number and width with increasing displacement (Figure 6). Additionally, cracks were observed at the ends of the beams, which eventually propagated into the beam-column joints at higher drift levels. This behavior occurred because a knee beam-column joint was used in the current study, which is prone to cracking due to the opening and closing of joints under lateral loads. The frame exhibited ductile behavior, and no shear failure was observed.

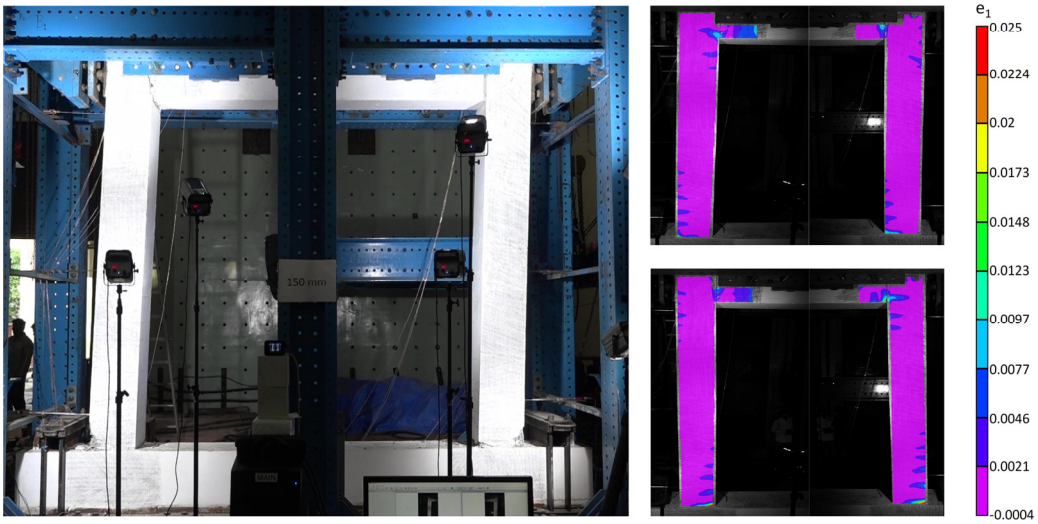

Figure 6: (a) Damage Pattern; and (b) Variation of Principal Strain in +ve and -ve Cycle at a Particular Drift for Bare Frame.

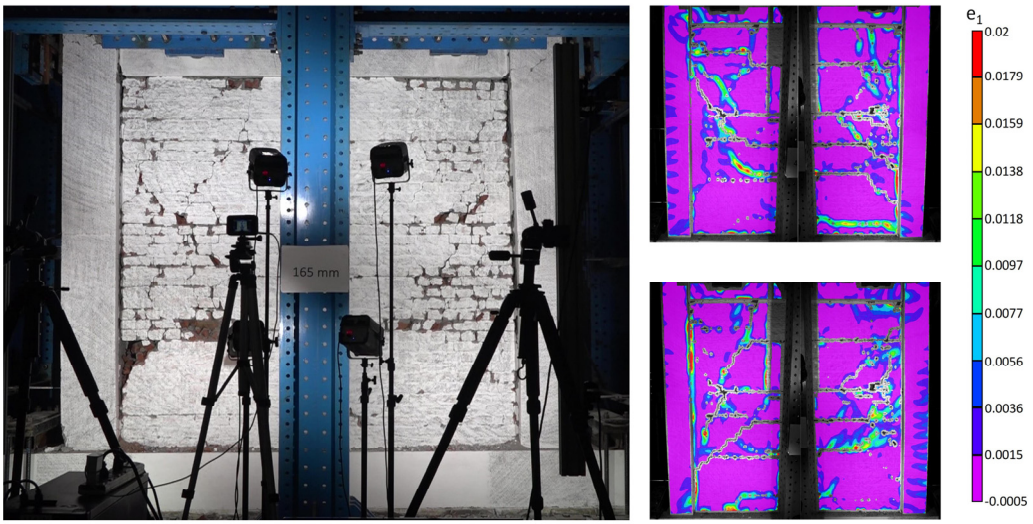

(a) (b)

Figure 7: (a) Damage Pattern; and (b) Variation of Principal Strain in +ve and -ve Cycle at a Particular Drift for Burnt Clay Brick Masonry Infilled Frame.

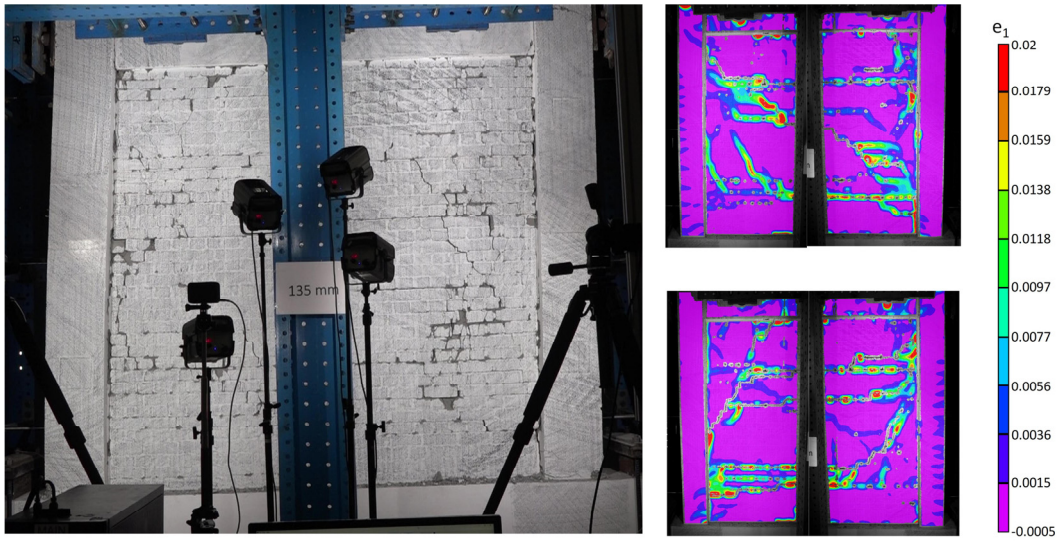

(a) (b)

Figure 8: (a) Damage Pattern; and (b) Variation of Principal Strain in +ve and -ve Cycle at a Particular Drift for Fly Ash Brick Masonry Infilled Frame.

For the burnt clay brick masonry infilled frame, initial cracks were observed at the top interface between the beam and the infill. With increasing displacement, diagonal cracks appeared, accompanied by bed joint sliding at mid-height (Figure 7). Vertical cracks were also observed along the column-infill interface. Spalling of masonry units began at a drift of 4%, and the infill completely collapsed at a drift of 6.25%.

For the fly ash brick masonry infilled frame, the primary failure mechanism was bed joint sliding, attributed to its lower bond strength (Figure 8). Cracks were also visible along the interface between the infill and the surrounding frame. After reaching a drift of 2%, cracks became widespread across the surface. Similar to

the burnt clay brick infill, the spalling of fly ash brick units started at a drift of 4%, with complete collapse occurring at 6.25%.

In the case of AAC block masonry infilled frame, a combination of bed joint sliding and diagonal cracking was observed (Figure 9). At larger displacements, the blocks began crushing at the corners due to their lower compressive strength. Eventually, the blocks began to detach from the infill at a drift of approximately 3.25% and ultimately collapsed at 5.5% drift.

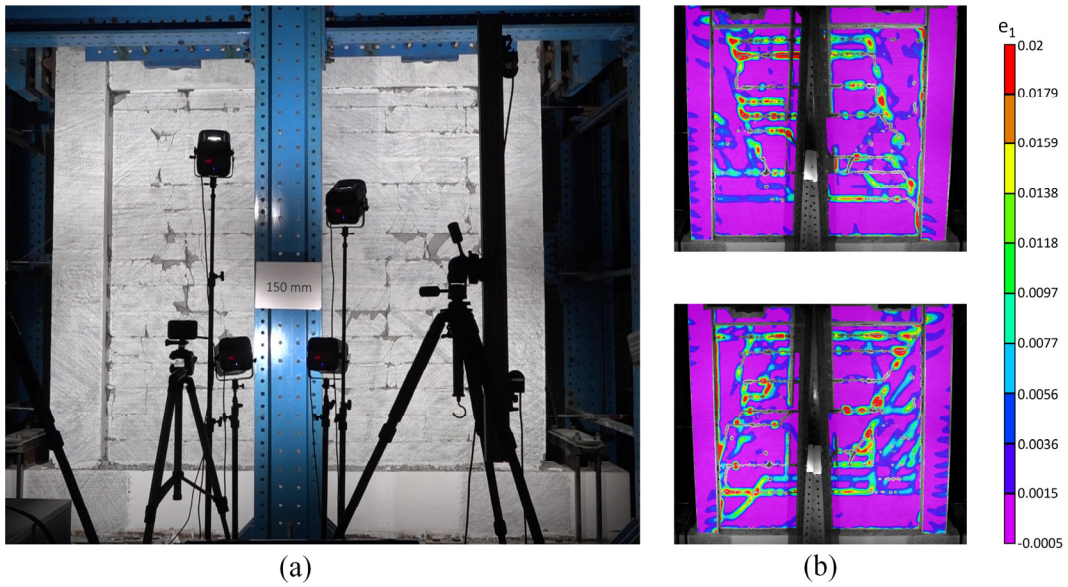

Figure 9: (a) Damage Pattern; and (b) Variation of Principal Strain in +ve and -ve Cycle at a Particular Drift for AAC Block Masonry Infilled Frame.

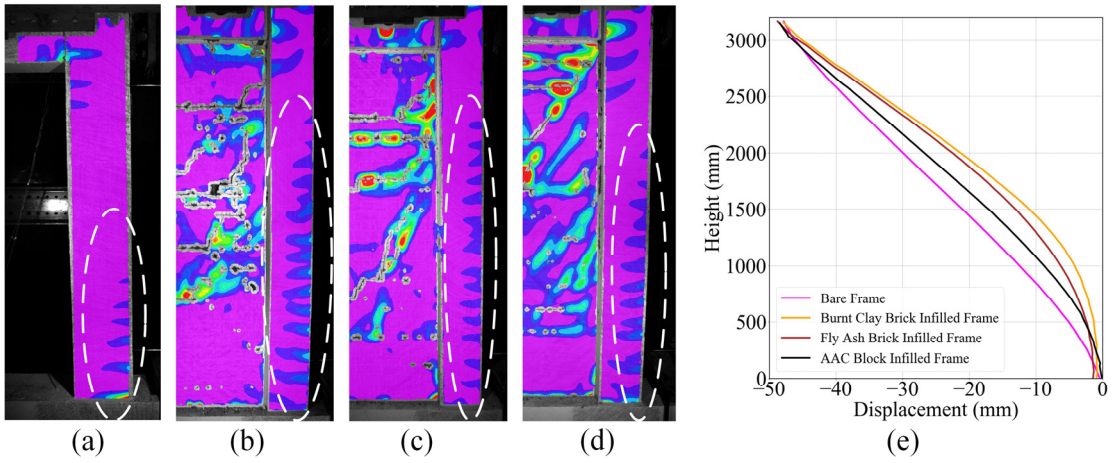

Figure 10: Flexure Crack Distribution in: (a) Bare Frame; (b) Burnt Clay Brick Masonry Infilled Frame; (c) Fly Ash Brick Masonry Infilled Frame; (d) AAC Block Masonry Infilled Frame; and (e) Variation of Lateral Displacement Along the Height of One of the Columns of the Specimens.

Figures 10(a–c) show the distribution of flexural cracks in one of the columns for all tested specimens. It can be observed that flexural cracks were more evenly distributed along the height of the columns in the

masonry infilled frames compared to the bare frame. This uniformity is attributed to the restraining effect of the infill, which limited lateral displacement at the column's base. This restraint effectively altered the column's effective length, leading to a more even distribution of cracks. Figure 10(c) illustrates the variation in lateral deformation along the column height for each specimen. The deformation was constrained up to a certain height, determined by the strength of the infill material. Among the infills, the burnt clay brick masonry provided the greatest restraint, while the AAC block masonry offered the least.

Comparison With the Analytical Models

The experimental results from this study were compared with existing analytical models that describe the behavior of masonry infills. For seismic assessments of masonry infilled RC frame structures, the behavior of infills is often modeled using single or multi-strut diagonal elements. This method is widely used due to its simplicity and computational efficiency. Here, the comparisons were focused on analytical models employing the single-strut approach. Various models are available in the literature to describe the behavior of single-strut models in terms of strength and stiffness [19-28]. Detailed descriptions of these models can be found in Bhat et al. [17].

Figure 11 presents a comparison of experimental and analytical results. For stiffness predictions, the model proposed by Huang et al. [24] showed satisfactory agreement with experimental data. In contrast, the models by Mainstone [22] and FEMA 1998 [23] underestimated the stiffness values, while all other models overestimated them. Regarding strength, the results showed good agreement with the predictions of ASCE 2017 [19]. Variations in predictions from other models were primarily attributed to the inherent uncertainties in material properties. In summary, while certain models provided accurate predictions for either stiffness or strength, none were capable of reliably estimating both parameters simultaneously. This underscores the need for more robust and comprehensive models that can better capture the variability in properties and behavior across different masonry types.

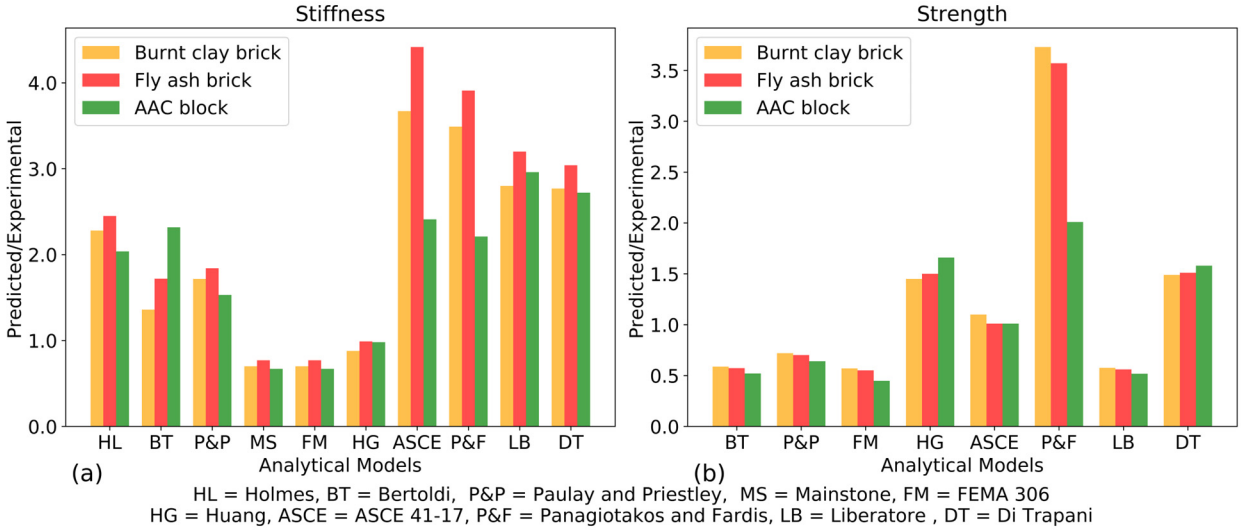

Figure 11: Ratio of Value Predicted Analytically to Experimental Values for (a) Stiffness; and (b) Strength.

CONCLUSIONS

Four full-scale RC frames, infilled with different types of masonry materials (burnt clay bricks, fly ash bricks, and AAC blocks), were subjected to in-plane quasi-static cyclic loading to evaluate the influence of these infills on strength, stiffness, and energy dissipation. Additionally, the impact of the updated design

provisions for RC frames in the current Indian seismic codes on the performance of infilled frames was assessed. Detailed crack propagation and infill-frame interaction were analyzed using Digital Image Correlation (DIC).

The masonry infilled frames demonstrated superior performance compared to the bare frame, achieving higher strength, stiffness, and energy dissipation. The strength of the burnt clay brick, fly ash brick, and AAC block infilled frames was found to be 1.8, 1.84, and 1.5 times greater, respectively, than that of the bare frame. Similarly, their initial stiffness was approximately 12.8, 10, and 7 times higher, respectively, than the bare frame.

Both the bare frame and the masonry infilled frames exhibited ductile failure modes, with no instances of shear failure observed in any of the specimens. This suggests that RC frames designed according to the current Indian seismic codes are capable of withstanding the lateral forces imposed by masonry infills without experiencing shear failure in the surrounding structural components.

In the masonry infilled frames, flexural cracks in the columns were more evenly distributed along the height compared to the bare frame. This behavior was attributed to the restraining effect of the infills, which limited lateral column deformation up to a certain height from the base.

Experimental findings showed a reasonable agreement with some analytical models in terms of either strength or stiffness individually. The correlation between experimental and predicted vaues of strength and stiffness was relatively better in case of AAC block masonry infills. However, no model was able to predict both parameters accurately. To address this limitation, probabilistic modeling offers a promising alternative for more comprehensive predictions.

ACKNOWLEDGEMENTS

This study was funded by NBCC (India) Limited and the Ministry of Human Resource Development (MHRD), which provided a research assistantship to the first author. The authors gratefully acknowledge their support.

REFERENCES

[1] Barbosa, A.R., Fahnestock, L.A., Fick, D.R., Gautam, D., Soti, R., Wood, R., Moaveni, B., Stavridis, A., Olsen, M.J., Rodrigues, H. (2017). Performance of medium-to-high rise reinforced concrete frame buildings with masonry infill in the 2015 Gorkha, Nepal, earthquake, *Earthq. Spctra* 33(1_suppl) 197-218.

[2] De Luca, F., Verderame, G.M., Gómez-Martínez, F., Pérez-García, A. (2014). The structural role played by masonry infills on RC building performances after the 2011 Lorca, Spain, earthquake, *Bull. Earthquake Eng.* 12 1999-2026.

[3] Decanini, L.D., De Sortis, A., Goretti, A., Liberatore, L., Mollaioli, F., Bazzurro, P. (2004). Performance of reinforced concrete buildings during the 2002 Molise, Italy, earthquake, *Earthq. Spctra* 20(1_suppl) 221-255.

[4] Fikri, R., Dizhur, D., Walsh, K., Ingham, J. (2019). Seismic performance of reinforced concrete frame with masonry infill buildings in the 2010/2011 Canterbury, New Zealand earthquakes, *Bull. Earthquake Eng.* 17 737-757.

[5] Manfredi, G., Prota, A., Verderame, G.M., De Luca, F., Ricci, P. (2014). 2012 Emilia earthquake, Italy: reinforced concrete buildings response, *Bull. Earthquake Eng.* 12 2275-2298.

[6] Perrone, D., Calvi, P., Nascimbene, R., Fischer, E., Magliulo, G. (2019). Seismic performance of non-structural elements during the 2016 Central Italy earthquake, *Bull. Earthquake Eng.* 17 5655-5677.

[7] Ricci, P., De Luca, F., Verderame, G.M. (2011). 6th April 2009 L'Aquila earthquake, Italy: reinforced concrete building performance, *Bull. Earthquake Eng.* 9 285-305.

[8] Sezen, H., Whittaker, A., Elwood, K., Mosalam, K. (2003). Performance of reinforced concrete buildings during the August 17, 1999 Kocaeli, Turkey earthquake, and seismic design and construction practise in Turkey, *Eng. Struct.* 25(1) 103-114.
[9] Varum, H., Furtado, A., Rodrigues, H., Dias-Oliveira, J., Vila-Pouca, N., Arêde, A. (2017). Seismic performance of the infill masonry walls and ambient vibration tests after the Ghorka 2015, Nepal earthquake, *Bull. Earthquake Eng.* 15 1185-1212.
[10] Verderame, G.M., De Luca, F., Ricci, P., Manfredi, G. (2011). Preliminary analysis of a soft-storey mechanism after the 2009 L'Aquila earthquake, *Earthq. Eng. Struct. Dyn.* 40(8) 925-944.
[11] Vicente, R.S., Rodrigues, H., Varum, H., Costa, A., Mendes da Silva, J.A.R. (2012). Performance of masonry enclosure walls: lessons learned from recent earthquakes, *Earthq. Eng. Eng. Vib.* 11 23-34.
[12] BIS (2000). Indian standard plain and reinforced concrete—Code of practice., IS 456, Bureau of Indian Standards, New Delhi, India.
[13] BIS (2016). Indian standard ductile detailing of reinforced concrete structures subjected to seismic forces–Code of practice., IS 13920, Bureau of Indian Standards, New Delhi, India.
[14] ACI (2013). Guide for testing reinforced concrete structural elements under slowly applied simulated seismic loads, ACI 374.2R-13, American Concrete Institute, Detroit, MI.
[15] Yoneyama, S. (2016). Basic principle of digital image correlation for in-plane displacement and strain measurement, *Advanced Composite Materials* 25(2) 105-123.
[16] Correlated Solutions.(2020). Vic-3D 9 Manual and Testing Guide, Correlated Solutions, Columbia.
[17] Bhat, Z.M., Singh, Y., Agarwal, P. (2024). Cyclic testing and diagonal strut modelling of different types of masonry infills in reinforced concrete frames designed for modern codes, *Eng. Struct.* 317(C) 118695.
[18] Bhat, Z.M., Singh, Y., Agarwal, P. (2023). Characterization of mechanical behavior of different types of masonry with a detailed investigation of full-field strain using digital image correlation, *Constr Build Mater.* 407 133502.
[19] ASCE (2017). Seismic evaluation and retrofit of existing buildings, ASCE/SEI 41-17, American Society of Civil Engineers, Reston, Virginia.
[20] Holmes, M. (1961). Steel frames with brickwork and concrete infilling, *Proceedings of the Institution of civil Engineers* 19(4) 473-478.
[21] Bertoldi, S., Decanini, L., Gavarini, C. (1993). Telai tamponati soggetti ad azioni sismiche, un modello semplificato: confronto sperimentale e numerico, *Atti del* 6(Oct) 815-824.
[22] Mainstone, R.J. (1974) Supplementary note on the stiffnesses and strengths of infilled frames, Building Research Establishment, Building Research Station.
[23] FEMA (1998). Evaluation of Earthquake Damaged Concrete and Masonry Wall Buildings—Basic Procedures Manual., FEMA 306, Federal Emergency Management Agency, Washington D.C.
[24] Huang, H., Burton, H.V., Sattar, S. (2020). Development and utilization of a database of infilled frame experiments for numerical modeling, *J. Struct. Eng.* 146(6) 04020079.
[25] Paulay, T., Priestley, M.N. (1992) Seismic design of reinforced concrete and masonry buildings, Wiley New York.
[26] Liberatore, L., Noto, F., Mollaioli, F., Franchin, P. (2018). In-plane response of masonry infill walls: Comprehensive experimentally-based equivalent strut model for deterministic and probabilistic analysis, *Eng. Struct.* 167 533-548.
[27] Di Trapani, F., Bertagnoli, G., Ferrotto, M.F., Gino, D. (2018). Empirical equations for the direct definition of stress–strain laws for fiber-section-based macromodeling of infilled frames, *J. Eng. Mech.* 144(11) 04018101.
[28] Panagiotakos, T., Fardis, M.(1996). Seismic response of infilled RC frames structures, 11th world conference on earthquake engineering, Acapulco, Mexico.